HHS Public Access

Author manuscript

Adv Mater. Author manuscript; available in PMC 2019 March 01.

Published in final edited form as:

Adv Mater. 2018 March ; 30(10): . doi:10.1002/adma.201704189.

Electrically Driven Microengineered Bio-inspired Soft Robots

Dr. Su Ryon Shin[†,*],
Biomaterials Innovation Research Center, Division of Engineering in Medicine, Brigham and Women's Hospital, Harvard Medical School, Boston, MA 02139, USA

Harvard-MIT Division of Health Sciences and Technology, Massachusetts Institute of Technology, Cambridge, MA 02139, USA

Dr. Bianca Migliori[†],
Biomaterials Innovation Research Center, Division of Engineering in Medicine, Brigham and Women's Hospital, Harvard Medical School, Boston, MA 02139, USA

Harvard-MIT Division of Health Sciences and Technology, Massachusetts Institute of Technology, Cambridge, MA 02139, USADepartment of Neuroscience, Karolinska Institutet, 17177 Stockholm, Sweden

Dr. Beatrice Miccoli,
Biomaterials Innovation Research Center, Division of Engineering in Medicine, Brigham and Women's Hospital, Harvard Medical School, Boston, MA 02139, USA

Harvard-MIT Division of Health Sciences and Technology, Massachusetts Institute of Technology, Cambridge, MA 02139, USADepartment of Electronics and Telecommunication, Politecnico di Torino, Torino, 10129, Italy

Dr. Yi-Chen Li,
Biomaterials Innovation Research Center, Division of Engineering in Medicine, Brigham and Women's Hospital, Harvard Medical School, Boston, MA 02139, USA

Harvard-MIT Division of Health Sciences and Technology, Massachusetts Institute of Technology, Cambridge, MA 02139, USA

Dr. Pooria Mostafalu,
Biomaterials Innovation Research Center, Division of Engineering in Medicine, Brigham and Women's Hospital, Harvard Medical School, Boston, MA 02139, USA

Harvard-MIT Division of Health Sciences and Technology, Massachusetts Institute of Technology, Cambridge, MA 02139, USA

Dr. Jungmok Seo,
Biomaterials Innovation Research Center, Division of Engineering in Medicine, Brigham and Women's Hospital, Harvard Medical School, Boston, MA 02139, USA

[*]S.R. Shin and A. Khademhosseini contributed equally as corresponding authors.
[†]S.R. Shin and B. Migliori contributed equally to this work.

Supporting Information
Supporting Information is available from the Wiley Online Library or from the author.

Harvard-MIT Division of Health Sciences and Technology, Massachusetts Institute of Technology, Cambridge, MA 02139, USA

Serena Mandla,
Biomaterials Innovation Research Center, Division of Engineering in Medicine, Brigham and Women's Hospital, Harvard Medical School, Boston, MA 02139, USA

Harvard-MIT Division of Health Sciences and Technology, Massachusetts Institute of Technology, Cambridge, MA 02139, USA

Alessandro Enrico,
Biomaterials Innovation Research Center, Division of Engineering in Medicine, Brigham and Women's Hospital, Harvard Medical School, Boston, MA 02139, USA

Harvard-MIT Division of Health Sciences and Technology, Massachusetts Institute of Technology, Cambridge, MA 02139, USA

Silvia Antonia,
Biomaterials Innovation Research Center, Division of Engineering in Medicine, Brigham and Women's Hospital, Harvard Medical School, Boston, MA 02139, USA

Harvard-MIT Division of Health Sciences and Technology, Massachusetts Institute of Technology, Cambridge, MA 02139, USA

Ram Sabarish,
Biomaterials Innovation Research Center, Division of Engineering in Medicine, Brigham and Women's Hospital, Harvard Medical School, Boston, MA 02139, USA

Harvard-MIT Division of Health Sciences and Technology, Massachusetts Institute of Technology, Cambridge, MA 02139, USA

Ting Zheng,
Biomaterials Innovation Research Center, Division of Engineering in Medicine, Brigham and Women's Hospital, Harvard Medical School, Boston, MA 02139, USA

Harvard-MIT Division of Health Sciences and Technology, Massachusetts Institute of Technology, Cambridge, MA 02139, USA

Pirrami Lorenzo,
Department of Electronics and Telecommunication, Politecnico di Torino, Torino, 10129, Italy

Department of Electrical Engineering, Institute for Printing, University of Applied Sciences and Arts Western Switzerland, Fribourg, 1705, Switzerland

Kaizhen Zhang,
Department of Mechanical and Industrial Engineering, Northeastern University, Boston, Massachusetts 02115, USA

Dr. Yu Shrike Zhang,
Biomaterials Innovation Research Center, Division of Engineering in Medicine, Brigham and Women's Hospital, Harvard Medical School, Boston, MA 02139, USA

Harvard-MIT Division of Health Sciences and Technology, Massachusetts Institute of Technology, Cambridge, MA 02139, USA

Dr. Kai-tak Wan,
Department of Mechanical and Industrial Engineering, Northeastern University, Boston, Massachusetts 02115, USA

Dr. Demarchi Danilo,
Department of Electronics and Telecommunication, Politecnico di Torino, Torino, 10129, Italy

Dr. Mehmet R. Dokmeci, and
Biomaterials Innovation Research Center, Division of Engineering in Medicine, Brigham and Women's Hospital, Harvard Medical School, Boston, MA 02139, USA

Harvard-MIT Division of Health Sciences and Technology, Massachusetts Institute of Technology, Cambridge, MA 02139, USA

Prof. Ali Khademhosseini*
Biomaterials Innovation Research Center, Division of Engineering in Medicine, Brigham and Women's Hospital, Harvard Medical School, Boston, MA 02139, USA

Harvard-MIT Division of Health Sciences and Technology, Massachusetts Institute of Technology, Cambridge, MA 02139, USA

Nanotechnology Center, King Abdulaziz University, Jeddah 21569, Saudi Arabia

Department of Bioindustrial Technologies, College of Animal Bioscience and Technology, Konkuk University, Seoul 143-701, Republic of Korea

Keywords

Hydrogels; Flexible microelectrodes; Cardiac tissue engineering; Bio-inspiration; Bio-actuators

1. Introduction

Engineered living-synthetic systems with an ability to dynamically deform their shape and sense biological environments are of interest for various biomedical applications, such as building biorobots, biosensors, and artificial muscles.[1] In particular, to build these systems, a biological component is integrated on an artificial platform, and dynamically controlled by devices at the interface. The biological component provides functional capabilities, such as sensing or pulsing movements while the artificial substrate is used to ensure mechanical stability of the construct. Furthermore, the artificial substrate improves the functionality of the biological component, while ensuring good biocompatibility.[2] In addition, the integration of dynamic controls into the platform can potentially allow the manipulation of the robot over its direction and speed. It can also provide activation of certain patterns *via* stimulation to improve and control its efficiency during long-term operations. Among various biological components, there are many advantages in using living cells such as self-actuating cardiomyocytes, which can provide the autonomous contraction needed from the living systems to move. Therefore, the self-actuating cardiomyocytes have inspired the

development of biological cell-based machines, including muscular thin film-based bio-hybrid actuators,[2f] cantilevers,[2g] walking “biological bimorph” bio-bots,[2h, 2i] jellyfish-inspired robot,[2a] and self-propelled swimming robots.[2j] Despite the significant advances in this field, many limitations still remain, such as creating life-like movements, on-board control systems, autonomous control over direction, robust actuation, and low-power stimulation systems for the biorobots.

To overcome these limitations, bioengineers have borrowed inspiration from nature and concepts from materials/engineering community and have developed bio-inspired robots. These biorobot actuators are able to mimic, and even overcome the performance limitations of living organisms in some cases, thus opening new venues in biorobotics research. Moreover, natural mechanisms are generally self-sustaining, high-performance, and efficient with low-energy requirements, which are important factors that should be addressed to tackle the issues within the current technology.[3] Recently, Parker *et al*. have developed a phototactic, guided soft-robotic ray using optogenetic control of the cardiomyocytes cultured on an elastomeric material such as polydimethylsiloxane (PDMS) that replicated the overall batoid fish morphology and swimming behaviors (undulatory locomotion) such as stingrays and skates.[1b] However, despite the successful demonstration of the optogenetically controlled bio-inspired robots, optogenetic techniques have several limitations such as complicated development processes, long development times, potential toxicity of optogenetic tools at very high expression levels or long-term expression to decrease light powers and increase duty cycles and stability.[4] As an alternative to optogenetic technique, flexible microelectrodes are promising candidates to be easily or simply integrated to locally stimulate the cells/tissues and to provide control over the bio-inspired robots.[2f, 5] These flexible microelectrodes have favorable biocompatibility, high durability, long-term stimulation ability, and simplicity of fabrication process compared to the optogenetic techniques.

To create a bio-inspired soft robot with flexible microelectrodes, batoid fish can be a good model organism with several advantages as suggested in previous studies.[1b, 6] The batoid fish, which are cartilaginous fish with dorsoventrally flattened bodies and extended pectoral fins, can be easily mimicked by simplifying its structure and movements among various living organisms in the ocean. In addition, the flexible microelectrodes are amenable for easy integration into flattened bio-inspired robots. However, various batoid fish exhibit different swimming styles that largely depend on their skeletal architecture (e.g., cartilage joint patterns), along with their aligned muscle tissues on their pectoral fins.[6a] To create a natural motion, we intended to mimic the alignment of skeletal and muscular architecture of the batoid fish, in particular a stingray, which can modulate the movement of the robot in a biomimetic manner. Especially, the cartilage structure and arrangement are key criteria to consider in the design of an effective bio-inspired soft robot as it will have a strong influence on the kinematic motion of the robot. Therefore, to mimic the features of a stingray, the use of extracellular matrix (ECM)-based hydrogels could facilitate better organization of the cells on the substrate and allow for large deformation of robots with a greater degree of freedom than micro-patterned PDMS substrates. In contrast, the micro-patterned PDMS substrates have been known to affect the contractile behavior of cardiac tissue/cells due to its high substrate rigidity.[7] Furthermore, creating anisotropically contractile cardiac muscle to

provide the beating patterns and pumping motion, is a key engineering and scientific challenge with immense potential. As such, cells cultured on the substrate need to have the desired orientation and elongation. These properties can be realized using micropatterning method. Hence, microengineering approaches combined with ECM-based hydrogels can be used to create anisotropic tissue constructs to develop biomimetic robots in a convenient, rapid, precise, reliable, and inexpensive manner.[8]

To create this robot, an engineered scaffold was designed by drawing inspiration from the biomechanical model of a stingray with multi-layered structure composed of two different hydrogels such as polyethylene glycol (PEG) and carbon nanotubes (CNTs)-gelatin methacryloyl (GelMA) hydrogels. The non-degradable, non-toxic, mechanically robust PEG hydrogel acts as the cartilage in the stingray body. In addition, the photocrosslinkable PEG hydrogel can be easily micro-patterned to mimic the cartilage joint patterns and modulate the movement of the robot compared with a thin PEG hydrogel. Furthermore, the gold (Au) microelectrode can be easily transferred and integrated to the PEG hydrogel layer without ancillary sacrificial layers, which was developed in our previous study.[9] In another previous work of ours, we reported a GelMA hydrogel scaffold with homogeneously incorporated CNTs, which was shown to improve tissue organization, and cell-to-cell electrical coupling.[2e] Cardiomyocytes cultured on the CNT-GelMA hydrogels were found to spontaneously beat faster than the cells cultured on pure GelMA, and maintained a stronger beating activity.[10] Therefore, the CNT-GelMA micro-patterned hydrogel layer can act as a suitable substrate for cell culture to induce rapid maturation of the cardiomyocytes. In addition, the encapsulation of nanomaterials, such as CNTs into the hydrogel was demonstrated to be a suitable method to provide the desired mechanical properties required to efficiently facilitate the integration of Au microelectrodes.[11] Challenges arise when developing a controllable soft robotics system, as electrical components are typically bulky, brittle and fragile, whereas bio-inspired robots have a high elasticity and low elastic modulus. Therefore, flexible Au microelectrodes were designed to deform in line with the bio-inspired soft robot without cracking or disrupting the polymeric layers and to generate pulses for localized electrical stimulation. Consequently, the muscle-like bio-inspired soft robot with the micro-patterned Au stimulation electrodes have excellent mechanical integrity and produce controllable motion under an electrical field provided by the integrated flexible microelectrodes.[2f, 5] Accordingly, in this paper, we focused on developing an integration system that incorporate multiple biomaterials, electronic components and live cells while mimicking the complex architecture of stingray itself by microfabrication techniques.

2. Results and Discussion

2.1 Design of the bio-inspired soft robot

We designed and fabricated a bio-inspired soft robot, which combined the mechanical and biological properties of a sting ray (Figure 1). The bio-inspired soft robot was composed of four layers: aligned muscle tissue, micro-patterned CNT-GelMA hydrogel, a flexible Au microelectrode, and a micro-patterned PEG hydrogel layer. The first layer, which aimed to mimic the structure and function of the cartilage joint patterns (blue dot in Figure 1a) of the skeletal architecture in a sting ray, was composed of a PEG micro-patterned hydrogel

(Figure 1b). In this case, the PEG micro-patterned hydrogel allowed for easy deformation of the construct under cell contraction and relaxation while maintain the mechanical stability of the whole structure when compared with a thin PEG hydrogel film.[12] For the second layer, a network of flexible Au microelectrodes was integrated into the scaffold to stimulate the robot with precise control and efficient electrical signal propagation across the robot. The Au microelectrodes with nanometer thickness were designed with a meander line pattern, which helped dissipate the physical stress of the metal electrode during muscle actuation when embedded in the scaffold.[13] The third layer was designed to mimic the directional muscle alignment against the cartilage joint patterns of the stingray. A CNT-GelMA micro-patterned hydrogel, which acted at a biocompatible environment suitable for cardiomyocyte culture and alignment, was generated with a pattern perpendicular to the orientation to the PEG hydrogel pattern (Figure S1). Finally, the fourth layer consisted of neonatal rat cardiomyocytes seeded on top of the CNT-GelMA hydrogel pattern to obtain a sting ray-shaped bio-inspired soft robot. After the maturation of the cardiomyocytes, the CNT-GelMA hydrogel pattern ensured contractions in the direction of cell alignment while the PEG hydrogel pattern could release the membrane tension following contraction, thus allowing the scaffold to return to its original shape (Figure 1c and d). The detailed fabrication process of the bio-inspired soft robot with the incorporated flexible Au microelectrode is presented and schematically illustrated in the Supporting Information, Figure S1.

The spacing in between the microscale hydrogel patterns is an important factor affecting cell alignment and cell-cell interactions, as reported in a previous study.[14] Three different pattern distances were tested for both the PEG (200 μm, 300 μm, and 500 μm) and the CNT-GelMA (50 μm, 75 μm, and 150 μm) hydrogels. To optimize these parameters, we fabricated a two-layer micro-patterned structure, 50 μm in width and thickness, with the CNT-GelMA hydrogel layer residing on top of the PEG hydrogel layer. The resulting scaffold is shown in Figure 2a and b, where the uniformly patterned PEG and CNT-GelMA hydrogels perpendicular to the underlying patterns can be clearly identified. In addition, the density of hydrogel patterns on the same size of the resulting scaffold can be controlled by changing the spacing in between hydrogel patterns. The specific concentrations of GelMA (5 wt%) and CNT (1 mg/ml) were selected to improve the maturation of the cardiac muscle tissue and cell-cell electrical coupling based on our previous reports.[9b, 10a] As shown in the scanning electron microscopy (SEM) image (Figure 2c), the CNT-GelMA-patterned hydrogel layer showed both fibrous networks, which could be attributed to the crosslinking of the GelMA-coated CNTs *via* the acrylic groups, and porosity distribution on its surface. This network structure is similar to the physical characteristic of collagen fibers in the native ECM as GelMA is derived from gelatin, a degradation product of collagens.[10a] The fibrous network promoted cell retention, maturation, attachment, and myotube striation (Figure 2d).[10a] After cardiomyocyte seeding, interconnected networks with partial alignment in the direction of the hydrogel pattern were observed from the F-actin staining in the conditions of denser CNT-GelMA hydrogel patterns (50 and 75 μm). This small spacing allows the cells to adhere to and bridge the adjacent CNT-GelMA hydrogel patterns. On the contrary, clear and precise cell alignment on the CNT-GelMA hydrogel patterns was observed on scaffolds with 150-μm spacing because of the increased spacing between the hydrogel patterns (Figure 2e). Despite the inferior cell alignment, the spontaneous beating had higher rates and was more

stable on the patterns with 75-μm spacing (frequency: 0.9 ± 0.1 Hz) than on the ones with 50-μm spacing (frequency: 0.5 ± 0.2 Hz) and 150-μm spacing (frequency: 0.2 ± 0.1 Hz) (Figure 2f and g). This could be related to the higher number of cell-cell interactions, which led to the higher beating synchronization and rates.[15] The reported results are in agreement with our previous study, in which the beating behavior was highly correlated to the cellular connections and coupling.[10a] To perform powerful actuation though the alignment alone is not enough, as the cells need to be connected between each other to transmit the electric pulse and to actuate all at the same time. Therefore, our choice was narrowed down to the 50- and 75-μm spacing for the CNT-GelMA hydrogel pattern. The constructs with 50 μm of spacing resulted in a strong actuation, but the wings were not bending in the right direction resulting in an uncontrollable behavior. On the other hand, the constructs with 75 μm of spacing between CNT-GelMA patterns showed a powerful actuation and expected bending behavior. After identifying the 75-μm spacing as the optimal CNT-GelMA hydrogel pattern to induce strong beating behavior (Video 1), the cytotoxicity of the scaffold was further assessed, showing an increase in cell metabolic activity over a period of 7 days (Figure 2h). These results confirmed that the CNT-GelMA-patterned hydrogels were not cytotoxic to the cardiac cells and were capable of inducing proliferation of cardiac fibroblasts.

To increase the stability of the structure and to allow the soft robot to properly recover to its original shape after cardiomyocyte contraction, the concentration of the PEG hydrogel was optimized to 20 wt%. This choice represents a tradeoff between high-weight percent PEG hydrogels (>30 wt%), which were too stiff to allow for scaffold bending upon cell contraction, and low-weight percent PEG hydrogels (<10 wt%), which were unable to counteract the contractile cell traction forces that originate from actin polymerization and actomyosin interactions.[16] Therefore, this design was found to provide robust mechanical properties to increase the stability of the soft robot construct, while the micro-pattern of the PEG hydrogel allows for easy deformation of the construct under cell contraction and relaxation when compared to a thin PEG hydrogel film. Furthermore, the geometry of the supporting PEG hydrogel pattern dramatically affects the function of the bio-inspired soft robot in terms of both directional beating and overall structure folding. To prevent irreversible complete rolling of the soft robot during the dynamic beating of the cardiomyocytes, the pattern spacing of the PEG hydrogel support layer was varied between 200, 300, and 500 μm (Figure 2i). As expected, the pattern density of the PEG hydrogel strongly influenced the kinematics of the bio-inspired actuator. The bio-inspired actuator without PEG hydrogel pattern spontaneously rolled up and showed strong beating (Video 2). In the case of the 200-μm spacing, no folding of the overall structure was observed due to the high density of the PEG hydrogel pattern, which was too stiff to allow for the bending of the soft robot upon cardiomyocyte contraction (Video 3). On the contrary, a strong and irreversible rolling of the bio-inspired actuator was observed and showed weak beating behavior when the PEG hydrogel pattern had a spacing of 500 μm, thus compromising the actuation dynamics of the soft robot (Video 5). A middle ground for the PEG hydrogel pattern density was found to be at 300 μm. With this dimension, the supporting PEG hydrogel layer was soft enough to follow the cardiomyocyte-induced bending of the soft robot, while remaining sufficiently stable to prevent irreversible folding of the substrate. Therefore, we introduced a specific score index to evaluate the optimal spacing of both the

CNT-GelMA and PEG hydrogel layers to simultaneously obtain a strong synchronized beating behavior and prevent the irreversible rolling of the bio-inspired actuator (Figure 2i). The index consisted of the sum of a “rolling score” (0 in the case of no rolling, -1 in the case of rolling) and a “beating level” varying from 0, in the case of no beating, to 3, in the case of very strong beating behavior (Figure 2j). The highest score index was obtained for PEG and CNT-GelMA hydrogel patterns with spacing of 300 μm and 75 μm, respectively, which led to the optimal beating and actuation dynamics of the soft robot (Video 4).

2.2 Beating behavior of the cells on the scaffold

After seeding neonatal rat cardiomyocytes on the optimized soft robot with CNT-GelMA and PEG hydrogel patterns with distances of 75 μm and 300 μm, respectively, the cells were stained for cardiac-specific biomarkers, including sarcomeric α-actinin and connexin-43 (Cx-43)[17] to observe the tissue morphology and phenotypes. Notably, in the case of the 75-μm spacing CNT-GelMA hydrogel spacing, cardiomyocytes on the top layer were observed to show alignment along the CNT-GelMA hydrogel pattern, and were interconnected between the patterned lines (Figure 3a and b), leading to the formation of a pseudo-3D cardiac tissue construct. The obtained pseudo-3D cardiac tissue construct consisted of cardiomyocytes in layers, the (i-1 and -2) upper, (ii) middle, and bottom parts, based on aligned and random cardiomyocyte morphology. Both cell bodies and elongations were found to intrude the base and side CNT-GelMA hydrogel patterns (50 μm in width and thickness), which therefore served as pseudo-3D scaffolds instead of 2D substrates.[10a] More specifically, as shown in the schematic in Figure 3a, and confirmed by confocal fluorescent microscopy, a homogeneous distribution of Cx-43, and well-organized sarcomeric α-actinin structures were observed on the topmost tissue (Figure 3b (i-1 and -2) and Figure S2). This tissue is primarily responsible for the synchronous beating of the whole construct. Alternatively, in the middle and bottom parts sarcomeric α-actinin expression resulted in partially aligned and organized tissue along the muscle-like hydrogel structure (Figure 3b (ii)-(iii) and Figure S2), which was found to not only enhance the synchronous contractile properties of the structure but also to guide the actuation dynamics parallel to the direction of the CNT-GelMA hydrogel pattern (Figure 3a), inducing the swimmer-like movement of the bio-inspired soft robot.

The soft robot showed spontaneous and synchronous beating behavior when neonatal rat cardiomyocytes were cultured on the biomimetic scaffold starting at day 3 (beating frequency 1.0 ± 0.1 Hz) until day 9 (beating frequency 0.8 ± 0.1 Hz), with no significant reduction in beating rates (Figure 3c). Interestingly, because of the patterned design of the PEG hydrogel substrate, the cultured cardiomyocytes on the biomimetic multilayer scaffold showed a similar beating rate compared to those on pristine CNT-GelMA hydrogels as shown in our previous work.[10a] Consequently, the optimized micro-patterns on the PEG hydrogel did not inhibit the cardiac muscle actuation on the substrate. Moreover, the strong spontaneous beating behavior of the cardiomyocytes naturally induced the detachment of the scaffold from the supporting glass 4 or 5 days into the culture period, as shown in Figure 3d and Video 4. The rolling behavior of the edges on the lateral patterned fins was due to the cellular traction force along the CNT-GelMA hydrogel pattern, i.e., in the transverse direction.

Finally, the fabricated bio-inspired soft robot showed a unique self-actuating movement, but not yet forward propulsion. In Figure 3d and e, longitudinal (blue line, stretching) and transverse (green line, contracting) axes on the soft robot showed actuation in opposite directions at the same time. A much higher contraction of the laterally patterned fins was observed in the transverse axes of the soft robot due to the strong muscle contraction of the aligned cardiac tissue along the CNT-GelMA hydrogel patterns (Figure 3b (ii) and (iii)). In addition, the micro-pattern of the stiff PEG hydrogel with a spacing of 300 μm may help to induce the easy deformation of the micro-patterned soft CNT-GelMA hydrogel under cell contraction.

To confirm the mechanical properties of two micro-patterned hydrogels, we performed a nano-indentation test.[18] The Young's modulus, derived from the force indentation data using a Hertzian model, of the micro-patterned PEG hydrogel, was 651 ± 326 kPa, which was 30 times higher than that of the CNT-GelMA hydrogel (37 ± 16 kPa), as shown in Figure 3f. On the contrary, the soft robot showed less deformation in the longitudinal axes (blue dot line), i.e., in the direction of the PEG hydrogel pattern. The longitudinal displacement can be mainly attributed to the 60° angle of the CNT-GelMA pattern with respect to the main axes of the soft robot that induced a force component in the vertical direction (Figure 3g). Furthermore, the contraction of the topmost of the cardiac tissue (Figure 3b (i-1 and -2)) produced a stress on the underlying PEG hydrogel layer, which was relaxed by elongating in the opposite direction. This movement was more evident in the tail section due to the absence of the central body, which dampened the displacement due to higher stiffness of the PEG hydrogel. After one full contraction, the bio-inspired actuator returned to the original rest position because of the elastic response provided by the PEG hydrogel pattern. These assumptions were confirmed by the results of the actuation dynamics and the particle velocimetry analysis of the soft robot from 0 to 0.3 sec as shown in Figure 3d (ii).

To assess the ability to drive the contractions of the soft robot by electrical stimulation before integration of the microelectrode, a biphasic electrical pulse was applied to the soft robot to tune and artificially control the beating behavior through commercially available carbon rod electrodes as commonly reported in literature.[19] As outlined in Figure 3h, the overall beating frequency of the soft robot was controlled at different frequencies (0.5, 1, and 2 Hz), by stimulation through a biphasic pulse with a frequency equal to the target beating frequency, AC peak voltage amplitude between 0.5 V and 6 V, DC offset value of 0V, a fixed pulse width of 50 ms, and duty cycles of 2.5%, 5%, and 10% in cases of 0.5, 1.0, and 2.0 Hz, respectively. In addition, we observed decreased actuation amplitudes of the soft robot when the frequencies were increased. For example, when the soft robot was stimulated at a frequency higher than 0.5 Hz, the robot contracted due to the electrical stimulation before it completely relaxed since it did not have enough time to complete the full contraction cycle (contraction + relaxation) due to the inertia of the material. Furthermore, the soft robot showed a small delay in the actuation response when the applied frequency was higher. The contraction and relaxation force of the soft robot needs to counteract the stiffness of the scaffold. For this reason the actuation of the soft robot may not be able to precisely follow the applied frequency; however, still it was controllable for frequencies of up to 2 Hz.

2.3 Incorporation of Au microelectrodes to the scaffold

The local control of the electrical stimulation of the soft robot was achieved through the encapsulation of a set of 200 nm-thick Au microelectrodes in the structure. The Au microelectrodes (Figure 4a) were deposited on a glass substrate by e-beam evaporation (see the Experimental Section for further details). Atomic force microscopy (AFM) characterization (Figure 4b) revealed a root mean square (RMS) roughness of 2.0 ± 0.4 nm, therefore providing compelling evidence of the high quality of the deposited electrode. The shape of the embedded Au microelectrodes was designed to allow the structure to maintain a high degree of flexibility necessary for the microelectrodes to not impede the beating of cardiomyocytes, and to generate a uniform electric field distribution across the scaffold, such that a wave-like displacement (arc segment angles: 120°), originating from the central region of the structure can be achieved.

Direct UV crosslinking of the PEG and CNT-GelMA hydrogels on the surface of the microelectrodes not only prevented electrode delamination, but also allowed the microelectrodes to be directly incorporated between the two hydrogels. Successful transfer and encapsulation of the microelectrodes in the PEG hydrogels, was assessed using SEM (Figure 4c and 4d) to ensure that there were no cracks at the interface between the microelectrodes and the hydrogel or surface damage of the microelectrodes. The Au electrode was then completely enclosed in the micro-patterned CNT-GelMA hydrogel, which was assessed using optical imaging, as shown in Figure 4e. It was confirmed experimentally that the Young's modulus of the micro-patterned CNT-GelMA hydrogel on the Au electrode was similar to that of the micro-patterned CNT-GelMA hydrogel only. Therefore, the CNT-GelMA hydrogel was successfully deposited on top of the Au microelectrodes; however, the Au electrode may have partially prevented crosslinking of the CNT-GelMA prepolymer under the microelectrodes since the opaque nature of the Au electrodes prevented the illumination crosslinking the material underneath them. Finally, we created a bio-inspired soft robot with embedded Au microelectrodes between the hydrogel layers as shown in Figure 4f. To further assess the stability of the electrodes in cell culture condition, its resistance was monitored for 5 days of incubation in cell culture media at 37 °C, (Figure 4g). Only a slight variation of resistance was observed during the 5 days of culture, thus confirming the stability and adhesiveness of the electrode in the biological environment.

In addition, the modulus of the electrical impedance was measured for the transferred microelectrodes on the PEG hydrogel layer, the encapsulated microelectrode within two hydrogel layers, and the entire soft robot with cultured cardiomyocytes (Figure 4h). As expected, at frequencies higher than 0.1 kHz, the presence of the capacitive current strongly decreased the modulus of the impedance on the PEG/microelectrodes (from 630 Ω to 251 Ω), PEG/microelectrodes/CNT-GelMA (from 280 Ω to 61 Ω) and PEG/microelectrodes/CNT-GelMA/cardiomyocytes (from 318 Ω to 89 Ω) samples between 0.1 and 82.5 kHz. Alternatively, at lower frequencies that are more representative of physiological conditions, an impedance modulus reduction could be observed when the CNT-GelMA hydrogel layer was added on the PEG/microelectrodes structure (from 2.3 kΩ to 1.6 kΩ at 0.1 Hz). This can be attributed to the presence of additional current paths through the CNTs incorporated in

the GelMA hydrogel, and would therefore contribute to an efficient electrical signal propagation through the cardiomyocytes. When cardiomyocytes were seeded on the soft robot with the embedded Au microelectrodes, a moderate impedance modulus increase was noticed, likely due to the intrinsic resistivity of the cells. Moreover, to confirm the organization of cardiac tissue on the microelectrodes-incorporated soft robot, immunostaining of sarcomeric α-actinin and F-actin was investigated. As shown in Figure 4i and 4j, we observed the random network formation of cardiac tissue with well-interconnected sarcomeric structures on the central body due to the absence of a pattern on the CNT-GelMA hydrogel. In addition, well-interconnected sarcomeric structures of cardiac tissues located directly above the microelectrodes were observed (Figure S3a). On the contrary, the cardiomyocytes were only partially aligned with the micro-patterned CNT-GelMA hydrogels on the laterally patterned fins, as evident from Figures 4k and 4l. In Figure S3 b and c, confocal fluorescence images showed well-elongated cardiac cells and well-developed F-actin cross-striations along with the CNT-GelMA hydrogel pattern.

2.4 Electrophysiological analysis of the bio-inspired actuator

After cardiomyocytes seeding, the bio-inspired construct with the embedded Au microelectrodes was able to efficiently maintain its original shape and integrity during the culture period. Moreover, to make use of the embedded microelectrodes, two copper wires were connected to the outermost end of the electrodes to electrically stimulate the bio-inspired actuator. The copper to Au attachment was insulated from the culture media by a thin layer of PDMS (Figure 4f). To investigate how an external voltage signal propagates and distributes *via* the embedded microelectrodes along the construct, finite element model simulations were performed using commercially available software (Comsol), both in the case of the embedded microelectrodes and the external carbon rod electrode. When a square wave signal (AC peak voltage amplitude 1V, DC offset value 0V, frequency 2.0 Hz, period 50 ms, duty cycle 10%) was applied in the case of the microelectrode stimulation, the maximum voltage intensity was found to be 1 V in the central area of the structure (Figure 4m). The observed non-uniform electric potential distribution suggested a non-spontaneous electrical excitation of the cardiomyocytes. This non-uniform electric potential distribution could generate the electrical propagation of the pulse conduction from one cell to another. Therefore, this can result in a wave-like displacement of the whole structure, in which the movement originates from the central body, and propagates towards the outer fin regions, mimicking the physiological actuation of the muscles to achieve defined contraction of the entire structure. On the contrary, the external carbon rod electrode simulation results revealed an almost uniform voltage distribution along the entire structure (Figure S4). This implies that the different areas of the scaffold would contract at the same time producing a defined on/off displacement, which is dissimilar to the movement of a sting ray. Moreover, during the simulation with the external carbon electrodes, the stimulation voltage peak was increased from 1 V to 4 V to take into account the signal attenuation in the cell culture media. As a result, the actual signal reaching the scaffold had peak amplitude of only 2 V, while, in the case of the microelectrode stimulation, the entire applied signal propagated through the core of the structure. This underlines how the local microelectrodes could offer improved stimulation efficiency.

To control the beating rates of the soft robot at a specific target frequency (0.5, 1.0, and 2.0 Hz), a biphasic pulse waveform at various frequencies (pulse width: 50 ms, duty cycle: from 2.5% to 10%, peak voltage amplitude: from 0.5 to 6 V, DC offset value: 0V, frequency: 0.5, 1.0, and 2.0 Hz) was applied to the microelectrodes. In the case of the external carbon rod electrodes, full synchronization was obtained with relatively low excitation peak voltages, ranging from 0.8 to 1.5 V (Figure S5). When the excitation frequency was increased from 0.5 to 2.0 Hz, the excitation threshold voltage also increased. This trend may be attributed to the slower actuation dynamics at the cellular level, which is limited by the repolarization and diffusion of nutrients from the ionic pumps. The same measurements were repeated in the case of local stimulation. The obtained excitation threshold voltage was slightly higher than the one obtained in the case of the external carbon rod electrode stimulation. Nevertheless, we successfully tuned the beating behavior of the cardiomyocytes at 0.5 and 1.0 Hz, as shown in Figure 4n. However, we were unable to achieve a stimulation frequency of 2.0 Hz, as the artificial tuning of the beating behavior could not be achieved for peak amplitudes smaller than 3 V, which was the maximum waveform amplitude we could apply. This indicates that much higher voltage amplitudes should be applied to the system.

The increase in the excitation threshold required for the embedded Au microelectrodes may be attributed to the simultaneous action of the two antagonist electrical phenomena. The first is that we expect the overall system resistance to increase with the embedded microelectrodes as a result of its smaller dimensions in comparison to the carbon electrodes. Second, during the local stimulation, the electrical signal was spatially closer, and almost coincident, with the cells rather than at a centimeter-scale distance away from the external electrodes. A smaller dielectric layer could thus be hypothesized in the case of embedded microelectrodes, i.e., a lower voltage drop between the electrode surface and the cells in favor of the effective potential present at the junction. Although the first effect should be predominant, the second could strongly contribute to mitigate it, maintaining the excitation threshold to relatively small values, of below 3 V, as experimentally observed. The tradeoff between these two phenomena allowed the embedded microelectrodes to efficiently and locally stimulate the bio-inspired soft robot. Finally, to evaluate the viability of cardiac tissues after local electrical stimulation, the spontaneous beating rates were recorded (Video 6). As shown in Figure 4o, the soft robot showed slightly different beating frequency until day 7 after the application of electrical stimulation with different parameters, performed for 4-5 h compared with that of the soft robot without microelectrodes and electrical stimulation. However, the overall beating frequency until day 7 was found to be around 1 Hz with strong spontaneous beating, which was very similar to the beating frequency of the soft robot without microelectrodes (Figure 3c). These results revealed that the microelectrode incorporation and the electrical tests produced only a negligible wear on the cell integrity, i.e., the beating behavior was still similar, and of the same order of magnitude to that observed when no electrode was present (Figure 3c). The obtained results strongly supported the concept that a bioinspired soft-robot could successfully control the beating rate using embedded Au microelectrodes without damaging the cardiac tissues.

In the pioneering work recently published by Parker *et al.* on a PDMS-based soft-robotic phototactic ray guided with optogentics[1b], they focused on the motion dynamics as opposed to mimicking the fish cartilage-muscle structure, which is nevertheless, the main

thrust of our work. In addition, our study has focused on developing an electrical stimulation system, instead of using genetically engineered cells with the optogenetic approach. Therefore, our method may eventually lead to the development of a wireless electrical stimulation system for production of bio-inspired soft robotics. Moreover, instead of PDMS, we selected a nanomaterial-incorporated hybrid hydrogel with the ability to simultaneously mimic the ECM components, while still having excellent electromechanical properties. The CNT-GelMA hydrogel is more favorable for cell proliferation and maturation, and allows for a more enhanced life-like actuation dynamics as a result of its softer properties. Naturally, both methods have their own merits, but the system we established with an embedded flexible microelectrode in the biomimetic hydrogel will offer an alternative strategy to move forward with the development of bioinspired soft-robots.

3. Conclusions

In summary, we have developed a bio-inspired soft robotics system, with integrated self-actuating cardiac myofibers on a hierarchically structured scaffold with flexible Au microelectrodes. The bio-inspired scaffold was sucessfully fabricated by mimicking the biomechanical model of a batoid fish, that is composed of two distinct micro-patterned hydrogel layers of PEG and CNTs-GelMA hydrogels. The cells were seeded on a CNT-GelMA hydrogel pattern overlying a PEG patterned hydrogel, with a Au microelectrode incorporated between the two materials. The bio-inspired scaffold showed good mechanical stability and ideal conditions for cell organization and maturation, as a result of the presence of ECM components in the CNT-GelMA hydrogel. High viability during cell seeding was followed by spontaneous beating behavior along the CNT-GelMA hydrogel pattern until day 7 of culture. Staining on day 5 revealed partial uniaxial alignment of sarcomeric α-actinin in the cells along the CNT-GelMA hydrogel pattern. The electrical stimulation of the bio-inspired actuator was performed using both external carbon rod electrodes as well as local embedded micrometer-size Au electrodes. Although local stimulation required higher excitation voltage thresholds with respect to external stimulation, in both cases it was possible to control the beating rates up to a frequency of 1.0 Hz, regardless of the natural beating rates of cells on the constructs, by applying peak voltages smaller than 3 V. Although our bio-inspired actuators do not generate forward propulsion, the results obtained in the present work not only encourage further developments in the field of bio-inspired actuators but also serve as an initial platform for new, cutting-edge studies on local electrical stimulation of cell-laden constructs with embedded microelectrodes for use as a wireless control system for the entire scaffold. Therefore, microfabricated cell-based hybrid actuators have the potential to greatly enhance the performance of biorobotics and potentially result in low-cost, fast, and easier-to-use analytical tools that are more portable and scalable for point-of-care sample analysis and real-time diagnostics. Furthermore, this proof of concept study even in absence of propulsion has potential applications in regenerative medicine e.g. cardiac or muscle patches integrated electrical stimulators for tissue regeneration.

4. Experimental section

Materials

The following reagents were purchased from Sigma-Aldrich (USA): Gelatin (Type A, 300 bloom from porcine skin), polyethylene glycol diacrylate (PEGDA) (M_W=1000), 3-(trimethoxysily) propyl methacrylate (TMSPMA), and methacrylic anhydride (MA). A carboxyl acid group functionalized multi-walled CNT (30 ± 15 nm in diameter and 5-20 μm length, 95% purity) was purchased from NanoLab Inc. The photo mask for the soft lithography and the shadow mask for the physical vapor deposition (PVD) process of the electrode patterning was purchased from CAD/Art Services, Inc. (USA) and from MINI MICRO STENCIL INC. (USA).

Preparation of the bio-inspired soft robot

The fabrication process is illustrated in Supporting Figure S1. First, the 200 nm-thick Au microelectrode with the desired wavy shape was fabricated on a glass substrate using the shadow mask by e-beam evaporation. In this process we did not include a Ti or Pt adhesion layers to facilitate the transfer process of the Au electrodes from the glass substrate to the hydrogel layer. Both the shadow mask for the Au microelectrode and the photomask used to fabricate the PEG and CNT-GelMA hydrogel patterns were designed using AutoCAD (Autodesk Inc., San Rafael, CA). The Au microelectrodes were then transferred onto the PEG hydrogel pattern by dispensing 10 μL of 20% PEG pre-polymer solution onto the Au microelectrode substrate, and TMSPMA coated glass was placed on top. The first photomask was interposed between the hydrogel and the UV light to produce the micro-pattern, and a spacer of 50 μm was placed between the electrode and the TMSPMA coated glass to produce a desired thickness of 50 μm for the PEG hydrogel layer. The pre-polymer solution was then cured by UV light (25.6 mW/cm^2) for 120 sec. By peeling the TMSPMA coated glass from the Au electrodes substrate, we successfully transferred the Au microelectrodes onto the micro-patterned PEG hydrogel substrate. The Au microelectrodes embedded in the micro-patterned PEG hydrogel was then placed on top of 20 μL of CNT-GelMA pre-polymer solution (with a 100 μm spacer) and UV crosslinked (25.6 mW/cm^2) for 240 sec with the second photomask. CNT-GelMA (1.0 mg/ml CNT in 5% GelMA) and PEG hydrogels were prepared based on our previously published reports.[10a, 20]

Characterization of the bio-inspired soft robot

A scanning electron microscope (SEM, Hitachi Model S4700, Japan) was used to assess the structure of the CNT-GelMA hydrogel. The samples were frozen in liquid nitrogen, then lyophilized, and finally coated with Pt/Pd using a sputter coater for SEM imaging. To measure the mechanical propertiesy of micro-patterned hydrogels, we performed AFM-assisted nano-indentation which was established in our published study.[21] The impedance modulus of the Au microelectrode at different intermediate fabrication steps was measured using an electrochemical workstation CHI660E (CH instrument, Inc.). We used an Ag/AgCl electrode as a reference electrode and Pt sheet as counter electrode along with Au microelectrode as the working electrode. For the electrochemical impedance spectroscopy technique, the initial potential was set to 0.1 V and the range of frequencies were scanned

from 0.1 Hz to 100 kHz at 5 mV of peak amplitude. All measurements were carried out in phosphate-buffered saline (PBS).

Cardiomyocytes isolation and culture

The cardiomyocytes were isolated from the heart ventricles of neonatal rats (2 days old Sprague-Dawley) following protocols approved by the Institute's Committee on Animal Care.[11c] The cells were cultured in Dulbecco's modified eagle medium (DMEM, ThermoFisher, USA) with 10% fetal bovine serum (FBS, ThermoFisher, USA), 1% L-glutamine, and 100 units/mL penicillin-streptomycin (ThermoFisher, USA).

Cell characterization

To access the viability of cardiomyocytes on the scaffold, an Alamar Blue assay (ThermoFisher, USA) was performed using the manufacturer's suggested protocol. The samples were analyzed on days 1, 3, 5, and 7 after cell seeding and the considered wavelength of absorption was 570 nm. For immunostaining, samples were fixed in 4% paraformaldehyde for 20 minutes and washed with PBS at room temperature. The samples were then treated in 0.15% Triton X-100 in PBS for 10 minutes. The samples were incubated with a cardiac biomarker (sarcomeric α-actinin and Cx-43 (Abcam, USA)) in the presence of a blocking buffer for 45 minutes at room temperature following the manufacturer's suggested dilution. Then, the samples were counterstained with DAPI (Sigma, USA) at a dilution of 1:1000 in PBS for an additional 20 minutes. The sample were also treated with Alexa Fluor 488 phalloidin (1:40 dilution in PBS) and DAPI for 40 minutes at room temperature. An inverted fluorescence microscope (Nikon, Eclipse TE 2000U, Japan) and an Inverted laser scanning confocal microscope (Leica SP5X MP, Germany) were used to obtain the cellular fluorescent images.

Actuation assessment of the bio-inspired soft robot

From day 1 to day 5, the bio-inspired actuators were incubated at 37 °C and imaged daily using an inverted optical microscope (Nikon, Eclipse TE 2000U, Japan). Once the cardiomyocytes began to show a beating activity (normally at day 3), the cell movements were recorded using video capture software at 20 frames per second (20 fps). By day 5, the bio-inspired actuator was detached from the TMSPMA coated glass. The sample was then placed in-between the two carbon rod electrodes spaced 3 cm apart in the culture media. The actuators were then stimulated by applying a square waveform with 50 ms pulses width, DC offset value 0V and a peak voltage amplitude between 0.5–6 V. The frequency was varied between 0.5, 1.0, and 2.0 Hz with a duty cycle between 2.5, 5 and 10%, respectively. The resulting beating activity was recorded using a commercially available camera. A custom developed MATLAB® code (MathWorks Inc., Natick, MA) was written to measure the bio-inspired actuator displacement along the selected directions. The local electrical stimulation *via* the Au microelectrode was carried out both for samples adhering to the glass substrate and for the detached samples. To deliver the electric signal directly on the internal Au electrode, two copper wires were attached to the Au electrode external square ports using silver paste. The silver paste was covered with a thin layer of PDMS pre-cured in the oven for 5 minutes. The PDMS was cured completely by placing the sample on a hotplate set at 45 °C for about 5 hours. The bio-inspired actuator was then electrically stimulated and tested

by applying a square wave with an offset voltage, V_{OFF}, set to 1 V and the amplitude, V_{ON}, was varied between 1.5 V and 5 V. For each of these conditions, stimulation frequencies of 0.5, 1.0, and 2.0 Hz were tested. The simulation of the propagation of the applied electrical signal through the structure with both the external and embedded Au microelectrodes was evaluated using COMSOL Multiphysics® electrostatic module (COMSOL Inc.), see Supporting Information for further details.

Statistical analysis

Statistical significance was performed by measuring one-way ANOVA tests (GraphPad Prism 5.02, GraphPad Software). To analyze and assess significant differences between selected treatments, Tukey's multiple comparison tests were utilized. Differences were characterized as significant for $p < 0.05$.

Supplementary Material

Refer to Web version on PubMed Central for supplementary material.

Acknowledgments

The authors declare no conflict of interests in this work. The authors gratefully acknowledge funding by the Defense Threat Reduction Agency (DTRA) under Space and Naval Warfare Systems Center Pacific (SSC PACIFIC) Contract No. N66001-13-C-2027. The authors also acknowledge funding from the National Institutes of Health (EB012597, AR057837, DE021468, HL099073, R56AI105024), the Presidential Early Career Award for Scientists and Engineers (PECASE), and Air Force Office of Sponsored Research under award # FA9550-15-1-0273. This work was partially supported by a microgrant from Brigham Research Institute and Center for Faculty Development and Diversity's Office for Research Careers at Brigham and Women's Hospital. S.R.S. would like to recognize and thank Brigham and Women's Hospital President Betsy Nabel, MD, and the Reny family, for the Stepping Strong Innovator Award through their generous funding. Y.S.Z. acknowledges supports from the National Cancer Institute Pathway to Independence Award (K99CA201603).

References

1. a) Holley MT, Nagarajan N, Danielson C, Zorlutuna P, Park K. Lab Chip. 2016; 16:3473. [PubMed: 27464463] b) Park SJ, Gazzola M, Park KS, Park S, Di Santo V, Blevins EL, Lind JU, Campbell PH, Dauth S, Capulli AK, Pasqualini FS, Ahn S, Cho A, Yuan H, Maoz BM, Vijaykumar R, Choi JW, Deisseroth K, Lauder GV, Mahadevan L, Parker KK. Science. 2016; 353:158. [PubMed: 27387948]
2. a) Nawroth JC, Lee H, Feinberg AW, Ripplinger CM, McCain ML, Grosberg A, Dabiri JO, Parker KK. Nature Biotechnology. 2012; 30:792.b) Herr H, Dennis RG. Journal of NeuroEngineering and Rehabilitation. 2004; 1c) Cvetkovic C, Raman R, Chan V, Williams BJ, Tolish M, Bajaj P, Sakar MS, Asada HH, Saif MTA, Bashir R. Proceedings of the National Academy of Sciences of the United States of America. 2014; 111:10125. [PubMed: 24982152] d) Kim J, Park J, Yang S, Baek J, Kim B, Lee SH, Yoon ES, Chun K, Park S. Lab on a Chip - Miniaturisation for Chemistry and Biology. 2007; 7:1504.e) Shin SR, Jung SM, Zalabany M, Kim K, Zorlutuna P, Kim SB, Nikkhah M, Khabiry M, Azize M, Kong J, Wan KT, Palacios T, Dokmeci MR, Bae H, Tang X, Khademhosseini A. ACS Nano. 2013; 7:2369. [PubMed: 23363247] f) Feinberg AW, Feigel A, Shevkoplyas SS, Sheehy S, Whitesides GM, Parker KK. Science. 2007; 317:1366. [PubMed: 17823347] g) Xi J, Schmidt JJ, Montemagno CD. Nat Mater. 2005; 4:180. [PubMed: 15654345] h) Chan V, Park K, Collens MB, Kong H, Saif TA, Bashir R. Sci Rep. 2012; 2:857. [PubMed: 23155480] i) Chan V, Jeong JH, Bajaj P, Collens M, Saif T, Kong H, Bashir R. Lab Chip. 2012; 12:88. [PubMed: 22124724] j) Williams BJ, Anand SV, Rajagopalan J, Saif MT. Nat Commun. 2014; 5:3081. [PubMed: 24435099]
3. Rus D, Tolley MT. Nature. 2015; 521:467. [PubMed: 26017446]

4. Tye KM, Deisseroth K. Nat Rev Neurosci. 2012; 13:251. [PubMed: 22430017]
5. Jia Z, Valiunas V, Lu Z, Bien H, Liu H, Wang HZ, Rosati B, Brink PR, Cohen IS, Entcheva E. Circ Arrhythm Electrophysiol. 2011; 4:753. [PubMed: 21828312]
6. a) Russo RS, Blemker SS, Fish FE, Bart-Smith H. Bioinspiration & biomimetics. 2015; 10:046002. [PubMed: 26079094] b) Li T, Li G, Liang Y, Cheng T, Dai J, Yang X, Liu B, Zeng Z, Huang Z, Luo Y, Xie T, Yang W. Sci Adv. 2017; 3:e1602045. [PubMed: 28435879]
7. McCain ML, Agarwal A, Nesmith HW, Nesmith AP, Parker KK. Biomaterials. 2014; 35:5462. [PubMed: 24731714]
8. a) Kane RS, Takayama S, Ostuni E, Ingber DE, Whitesides GM. Biomaterials. 1999; 20:2363. [PubMed: 10614942] b) Xia YN, Whitesides GM. Angewandte Chemie-International Edition. 1998; 37:551.c) Khademhosseini A, Jon S, Suh KY, Tran TNT, Eng G, Yeh J, Seong J, Langer R. Advanced Materials. 2003; 15:1995.d) Suh KY, Khademhosseini A, Yang JM, Eng G, Langer R. Advanced Materials. 2004; 16:584.e) Whitesides GM, Ostuni E, Takayama S, Jiang XY, Ingber DE. Annual Review of Biomedical Engineering. 2001; 3:335.
9. a) Tian B, Liu J, Dvir T, Jin L, Tsui JH, Qing Q, Suo Z, Langer R, Kohane DS, Lieber CM. Nat Mater. 2012; 11:986. [PubMed: 22922448] b) Shin SR, Shin C, Memic A, Shadmehr S, Miscuglio M, Jung HY, Jung SM, Bae H, Khademhosseini A, Tang XS, Dokmeci MR. Advanced Functional Materials. 2015; 25:4486. [PubMed: 27134620]
10. a) Shin SR, Jung SM, Zalabany M, Kim K, Zorlutuna P, Kim SB, Nikkhah M, Khabiry M, Azize M, Kong J, Wan KT, Palacios T, Dokmeci MR, Bae H, Tang XS, Khademhosseini A. ACS Nano. 2013; 7:2369. [PubMed: 23363247] b) Shin SR, Aghaei-Ghareh-Bolagh B, Gao X, Nikkhah M, Jung SM, Dolatshahi-Pirouz A, Kim SB, Kim SM, Dokmeci MR, Tang XS, Khademhosseini A. Adv Funct Mater. 2014; 24:6136. [PubMed: 25419209]
11. a) Dvir T, Timko BP, Brigham MD, Naik SR, Karajanagi SS, Levy O, Jin H, Parker KK, Langer R, Kohane DS. Nature Nanotechnology. 2011; 6:720.b) Shin SR, Bae H, Cha JM, Mun JY, Chen YC, Tekin H, Shin H, Farshchi S, Dokmeci MR, Tang S, Khademhosseini A. ACS Nano. 2012; 6:362. [PubMed: 22117858] c) Shin SR, Shin C, Memic A, Shadmehr S, Miscuglio M, Jung HY, Jung SM, Bae H, Khademhosseini A, Tang X, Dokmeci MR. Advanced Functional Materials. 2015; 25:4486. [PubMed: 27134620] d) Blum AS, Soto CM, Sapsford KE, Wilson CD, Moore MH, Ratna BR. Biosensors and Bioelectronics. 2011; 26:2852. [PubMed: 21185715] e) Rajzer I, Rom M, Menaszek E, Pasierb P. Materials Letters. 2014; 138:60.f) Baei P, Jalili-Firoozinezhad S, Rajabi-Zeleti S, Tafazzoli-Shadpour M, Baharvand H, Aghdami N. Materials Science and Engineering C. 2016; 63:131. [PubMed: 27040204]
12. a) Wang Y, Yang R, Shi Z, Zhang L, Shi D, Wang E, Zhang G. ACS Nano. 2011; 5:3645. [PubMed: 21452882] b) Sharifi S, Blanquer SB, van Kooten TG, Grijpma DW. Acta Biomater. 2012; 8:4233. [PubMed: 22995403]
13. Gutruf P, Walia S, Ali MN, Sriram S, Bhaskaran M. Appl Phys Lett. 2014:104.
14. Li YC, Lin MW, Yen MH, Fan SM, Wu JT, Young TH, Cheng JY, Lin SJ. ACS Appl Mater Interfaces. 2015; 7:22322. [PubMed: 26393271]
15. Lind JU, Busbee TA, Valentine AD, Pasqualini FS, Yuan H, Yadid M, Park SJ, Kotikian A, Nesmith AP, Campbell PH, Vlassak JJ, Lewis JA, Parker KK. Nat Mater. 2016; doi: 10.1038/nmat4782
16. Tan JL, Tien J, Pirone DM, Gray DS, Bhadriraju K, Chen CS. Proc Natl Acad Sci U S A. 2003; 100:1484. [PubMed: 12552122]
17. a) Liu Z, Li W, Ma X, Ding N, Spallotta F, Southon E, Tessarollo L, Gaetano C, Mukouyama YS, Thiele CJ. J Biol Chem. 2014; 289:29801. [PubMed: 25190801] b) Tchao J, Han L, Lin B, Yang L, Tobita K. Sci Rep. 2014; 4:6614. [PubMed: 25310989]
18. Shin SR, Bae H, Cha JM, Mun JY, Chen YC, Tekin H, Shin H, Farshchi S, Dokmeci MR, Tang X, Khademhosseini A. ACS Nano. 2012; 6:362. [PubMed: 22117858]
19. Tandon N, Cannizzaro C, Chao PH, Maidhof R, Marsano A, Au HT, Radisic M, Vunjak-Novakovic G. Nat Protoc. 2009; 4:155. [PubMed: 19180087]
20. Nichol JW, Koshy ST, Bae H, Hwang CM, Yamanlar S, Khademhosseini A. Biomaterials. 2010; 31:5536. [PubMed: 20417964]

21. Shin SR, Zihlmann C, Akbari M, Assawes P, Cheung L, Zhang K, Manoharan V, Zhang YS, Yuksekkaya M, Wan KT, Nikkhah M, Dokmeci MR, Tang XS, Khademhosseini A. Small. 2016; 12:3677. [PubMed: 27254107]

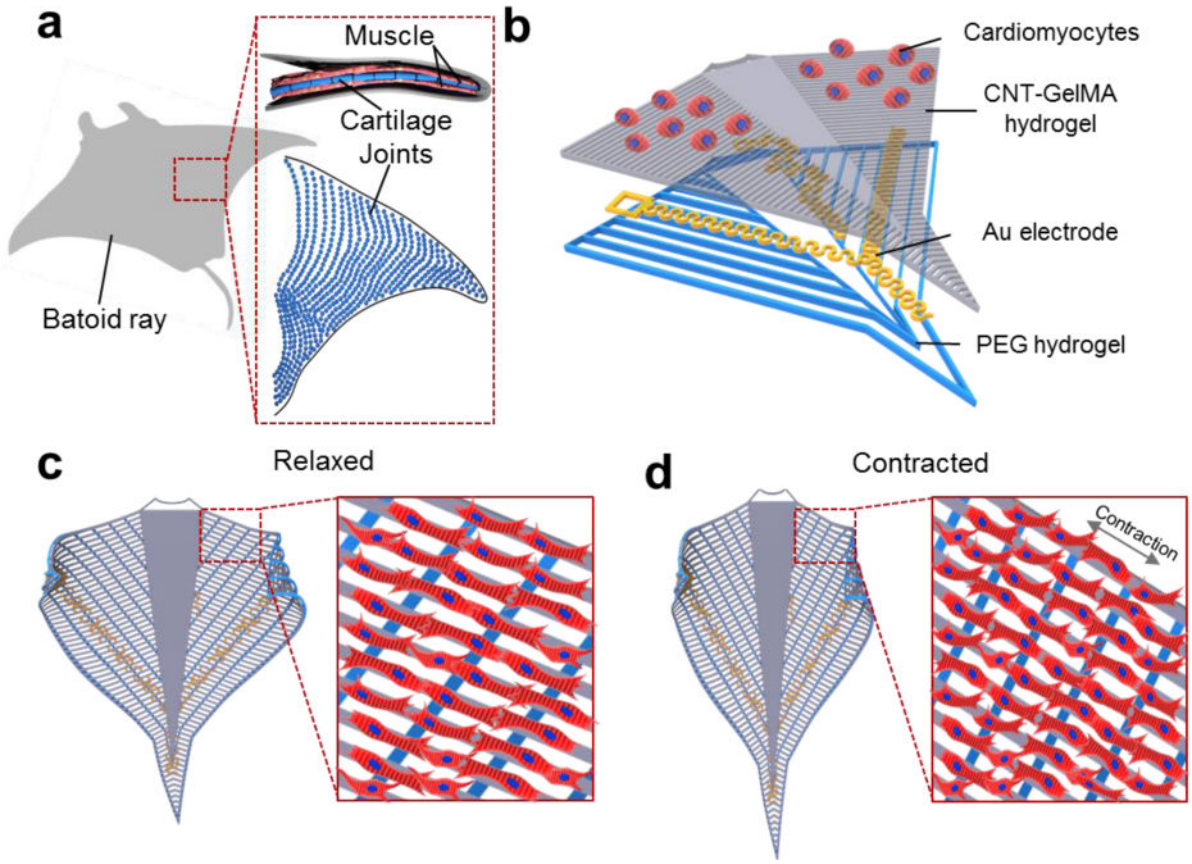

Figure 1. Schematic of the device

(a) Schematic of the cartilage joints and muscle patterns of a string ray. (b) Schematic illustration of the layer-by-layer structure of the construct. The bottom layer was composed of a PEG hydrogel with vertical line patterns for alignment. The upper layer in contact with the cells was made of patterned CNT-GelMA hydrogel with a pattern, which was perpendicular to the PEG hydrogel patterns. The microelectrodes were embedded in between the two layers. (c, d) Schematic design of the sting ray movement in the macro and micro scale: relaxed cardiomyocytes (c) and contracted cardiomyocytes (d).

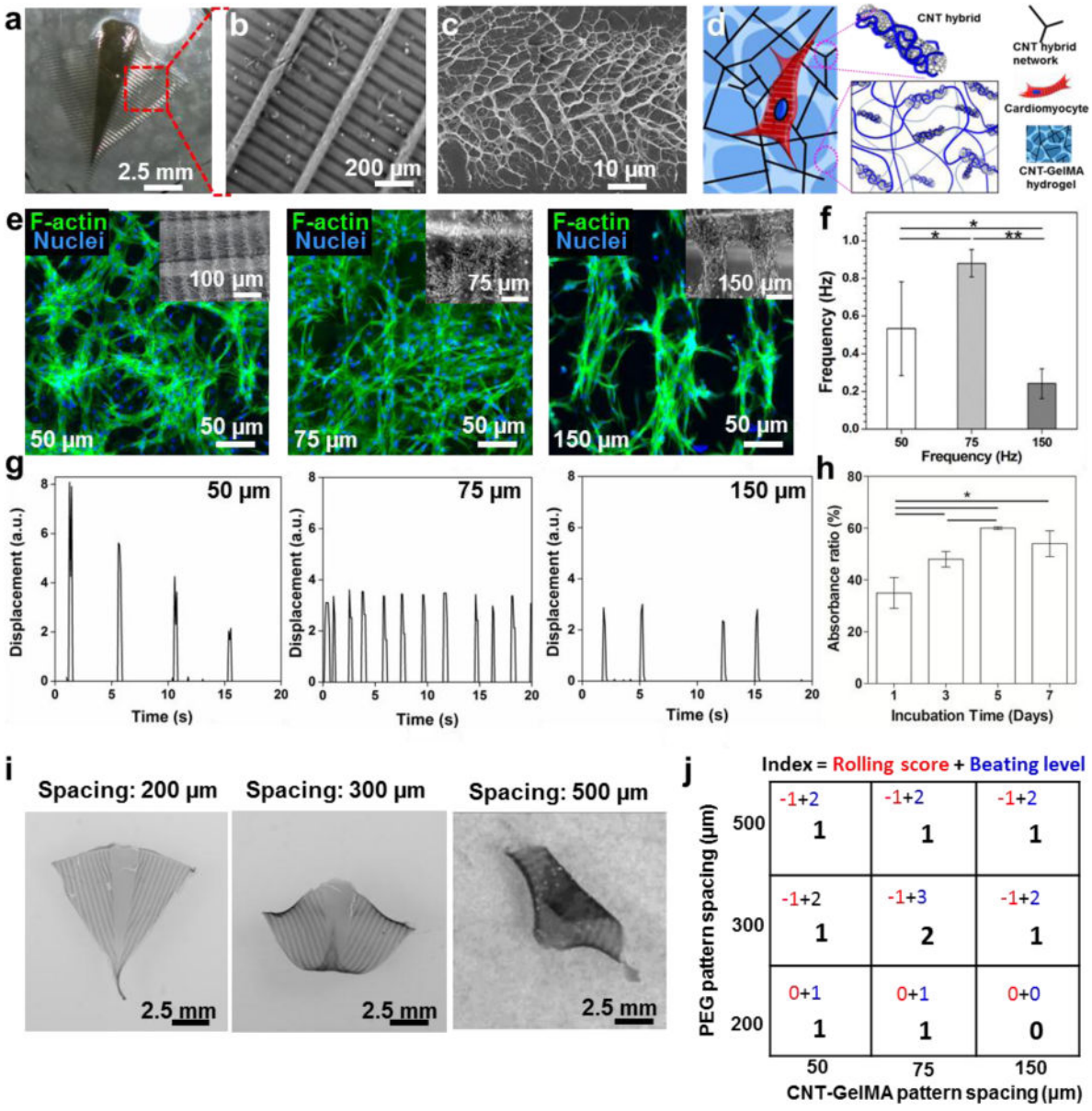

Figure 2. The optimization of PEG- and CNT-GelMA hydrogel patterns

(a) Image of the bio-inspired actuator without the Au microelectrode. (b) SEM image of the pattern of the dense CNT-GelMA hydrogel lines aligned perpendicular to the sparse PEG hydrogel lines. (c) SEM image of the fractal-like surface of the CNT-GelMA hydrogel pattern. (d) Schematic illustration of the CNTs embedded into the GelMA hydrogel. (e) Fluorescent images of cardiomyocytes on the CNT-GelMA hydrogel pattern with a 50-, 75-, and 150-μm spacing. (f) Spontaneous beating rates of cardiac tissues seeded on the multilayer bio-inspired actuator with different spacing between the CNT-GelMA hydrogel patterns on day 5. (*p< 0.05 and **p < 0.005) (h) Alamar blue assay of cardiomyocyte cultured on the bio-construct after 7 days of incubation revealed high cell viability. (*p < 0.05) (i) The rolling morphologies of the bio-inspired constructs with the PEG hydrogel pattern with a 200-, 300-, and 500-μm spacing. (j) Table showing the index of the PEG

hydrogel pattern and the CNT-GelMA hydrogel pattern optimization process: different spacings between the lines of PEG and CNT-GelMA hydrogel patterns have been inspected. For each device made with a different combination of patterns, the cell spreading, alignment, and beating behavior was analyzed. (Beating level indicated: 0, Very weak or no beating; 1, Weak beating; 2, Strong beating; 3, Very Strong beating. Rolling score indicated: -1, Rolling; 0, No Rolling).

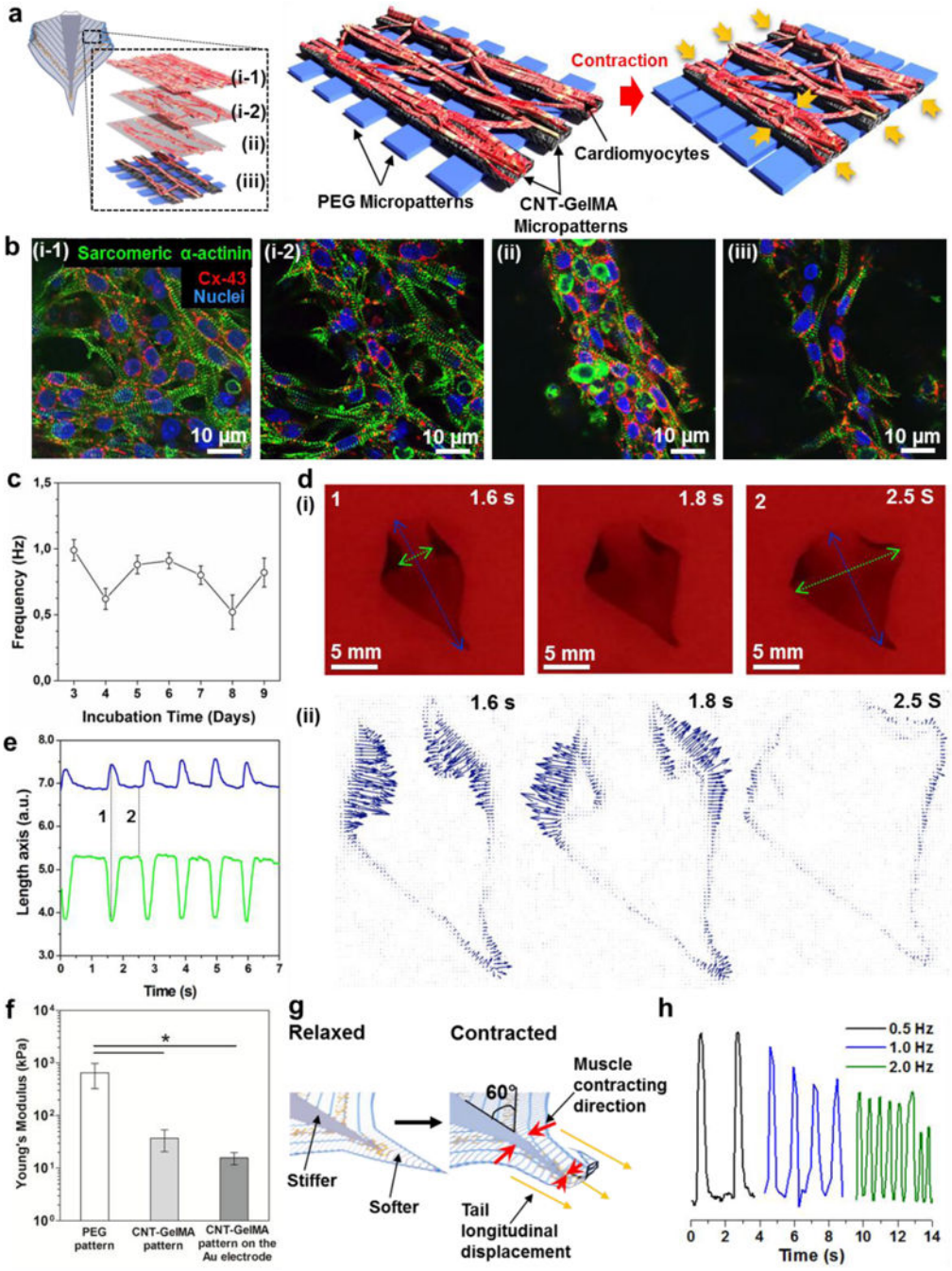

Figure 3. The characterization of the cardiomyocytes on the bio-inspired scaffold

(a) Schematic illustration of the contraction behavior of the cultured cardiac muscle tissue on the bio-inspired scaffold. The cultured cardiac muscle tissue showed a pseudo-3D structure, which could be separated into four layers, the (i-1 and -2) upper, (ii) middle, and (iii) bottom, based on aligned and random cardiomyocyte morphology. (b) Confocal fluorescent images showed different morphology in the (i-1 and -2) upper, (ii) middle, and (iii) bottom of cardiomyocytes cultured on the bio-inspired scaffold for day 5. (c) Spontaneous beating rates of the cardiomyocytes on the bio-inspired scaffold from day 3 to

day 9. (d) (i) Photograph of a free-standing bio-inspired soft robot cultured for 5 days at 0, 0.18, and 0.3 sec. The blue line represents the longitudinal axis displacement while the green line represents the transverse axis displacement. (ii) Particle Image Velocimetry measurement of the bio-inspired soft robot spontaneously moved within 0.3 sec. All arrows indicated direction and magnitude of the beating motion. (e) Displacement of the two major axes during stimulated contractions (2.0 Hz, 1 V/cm). The blue line represents the longitudinal axis displacement (corresponding to the blue line in Figure 3d) while the green line (corresponding to the green line in figure 3d) represents the transverse axis displacement. The frame taken in correspondence to the lines marked with 1 and 2 are shown in Figure 3d. (f) Young's modulus of the PEG hydrogel pattern, CNT-GelMA hydrogel pattern, and the CNT-GelMA hydrogel pattern fabricated on the Au microelectrode. (*$p < 0.05$) (g) Schematic of the mechanism of tail longitudinal displacement which induces the soft robot displacement along the vertical direction, mainly on the tail part, when the cells contract. (h) Beating response of the bio-inspired soft robot when stimulated with an AC external electrical field at 1V/cm and with various frequencies from 0.5 to 2.0 Hz.

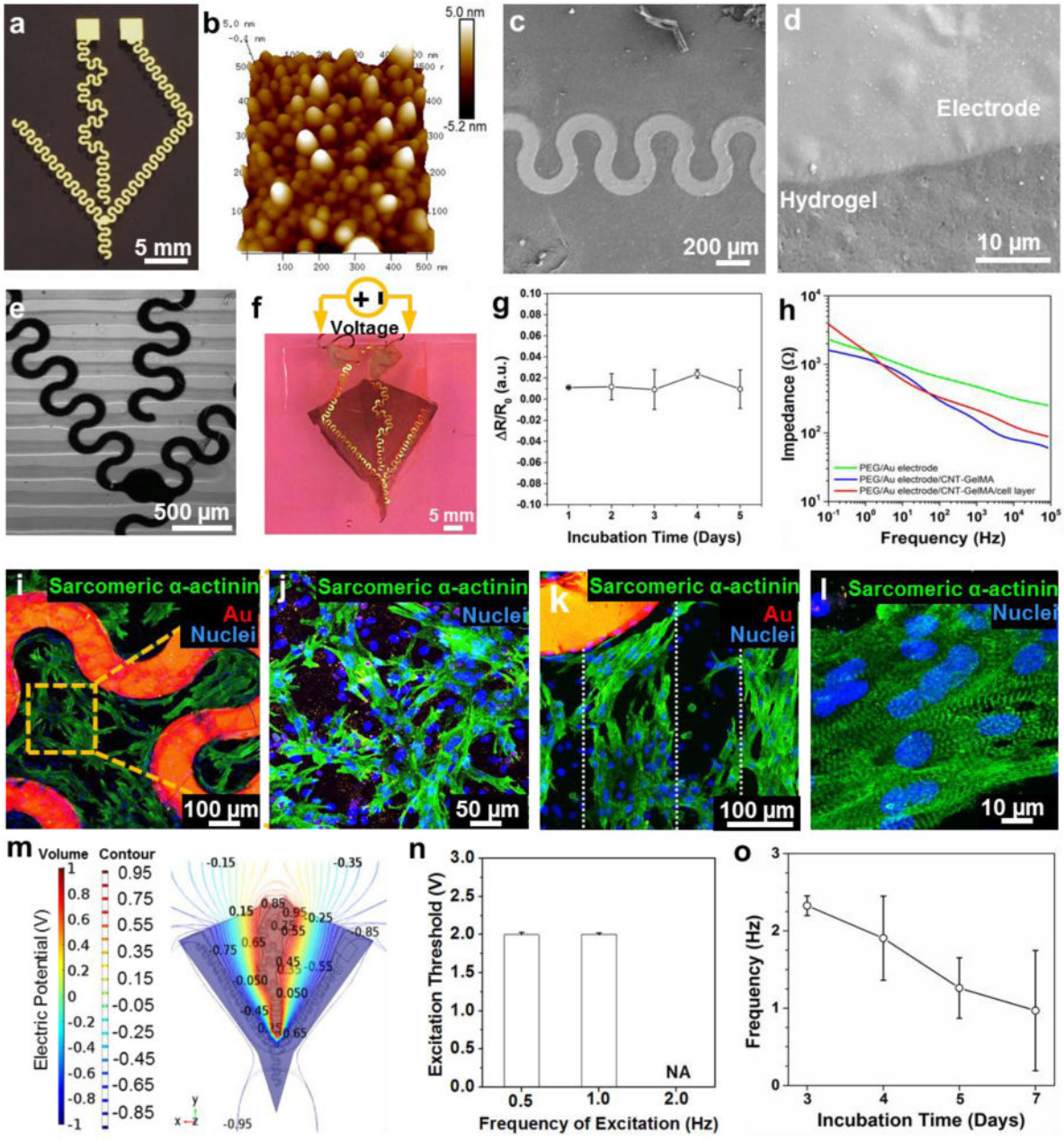

Figure 4. Characterization of the Au microelectrodes and their incorporation into the bio-inspired soft robot

(a) E-beam-evaporated Au microelectrodes with a serpentine pattern. (b) AFM image of the Au microelectrodes. (c) and (d) SEM image of the Au microelectrode successfully transferred onto the PEG hydrogel. (e) Optical microscope image of the Au microelectrodes successfully embedded in the CNT-GelMA hydrogel pattern. (f) Obtained bio-inspired soft robot with embedded Au microelectrodes. Copper wires were connected to the structure using silver paste to make an electrical contact for local electrical stimulation. (g) Variations in the Au microelectrodes resistance embedded in the bio-inspired scaffold during 5 days of incubation in cell culture media at 37 °C. (h) Measured impedance modulus of Au microelectrodes transferred on the PEG hydrogel pattern (green), embedded in between PEG

and CNT-GelMA hydrogel patterns (blue), and PEG and CNT-GelMA hydrogel patterns with cardiomyocytes layer (red). (i) Confocal fluorescence image of the cardiomyocytes, randomly spread among the Au microelectrodes (red signal) on the unpatterned central body. (j) The cardiomyocytes exhibited a random network organization on the unpatterned central body. (k) Well-elongated and aligned cardiomyocytes were showed on the CNT-GelMA hydrogel pattern which is indicated by the white dots. (l) Partial uniaxial sarcomere alignment and interconnected sarcomeric structure was observed on the patterned areas. (m) Top views of the numerically calculated electric potential contour plot volume distribution when a square wave signal (Peak Amplitude: 1 V, DC offset value: 0V, Frequency: 2.0 Hz, Pulse width: 50 ms, Duty Cycle: 10%) was applied to the embedded microelectrodes. (n) Excitation threshold voltage required at different frequencies (0,5, 1.0 and 2.0 Hz) when electrical stimulation was applied *via* the embedded Au microelectrodes. (o) Spontaneous beating behavior of the bio-inspired soft robot with embedded Au microelectrodes after electrical stimulation.